Blucher Mechanical Engineering Proceedings
May 2014, vol. 1 , num. 1
www.proceedings.blucher.com.br/evento/10wccm

A COMPUTATIONAL MODEL FOR STOCHASTIC WAVE PROPAGATION IN LONG STRUCTURES

Ruichong Zhang and Lotfi Gargab

Department of Civil and Environmental Engineering, Colorado School of Mines, Colorado, USA (rzhang@mines.edu)

Abstract. *This paper introduces a computational model for stochastic wave propagation in long structures of civil and mechanical engineering systems, exemplified as towers and pipelines, and characterized with one-dimensional waveguide materials inter-connected with lumped mass. The model can be used for predictive wave response analysis as well as for system identification and damage diagnosis in structural health monitoring.*

In this study, wave response at one location of the structure is derived to an impulsive motion at another location in time and frequency domains, termed here as wave-based or generalized impulse and frequency response functions. Not only does this study show vibration features in wave responses with the hybrid model, typically explainable and usable with discrete or multi-degree-of-freedom modeling. The model based responses also capture wave scattering features traditionally comprehensible with continuous modeling. The latter plays a major role in effectively detecting structural damage crack, stiffness degradation, and/or material non-linearity.

Two examples are presented with the use of the modeling. One is wave-based characterization of ten-story Millikan Library in Pasadena, California with the recordings of Yorba Linda earthquake of September 3, 2002. The other is analysis for influence of stochastic material/geometrical features in wave responses.

Keywords: *Wave-based approach, Seismic responses of buildings, System identification.*

1. INTRODUCTION

Response analysis and system identification of high-rise buildings with seismic excitation are typically carried out within the framework of vibration theory. In this vibration-based approach, the building structure is modeled as a discrete or a multi-degree-of-freedom (MDOF) system, and structural dynamic properties are characterized with modal frequencies and shapes that are a function of physical parameters such as floor mass and column/wall stiffness. Subsequently, seismic responses are obtainable for a given excitation, and system parameters are identifiable if seismic recordings are provided. Furthermore, structural nonlinear analysis and damage diagnosis are achievable by updating the linear MDOF model to nonlinear one. While this approach is widely used and capable in solving many issues raised in performance-based design and structural vibration control, it has limitation in characterizing comprehensive seismic motion in structures, subsequently affecting the broad-based applications such as effective identification of local system parameters or damage with a limited number of recordings.

The limitation of the vibration-based approach resides in the implicit assumption that seismic responses are synchronous at different locations of the structure. In fact, seismic responses are the result of wave propagation in large-scale structures such as high rise buildings or towers and multiply supported pipelines, in which some wave phenomena such as time delay of traveling waves from one location to the other plays an important role in in-depth understanding of seismic recordings and effective identification of local structural features (Kohler et al. 2007; Todorovska et al., 2001).

Recent studies show advantages of wave-based approach over vibration-based one in some seismic response analysis and damage diagnosis of building structures. In particular, Iwan (1996) proposed to use one-dimensional (1D) uniform shear-beam model for buildings and obtained seismic drift spectrum for design. Safak (1999) introduced 1D continuous modeling for structure-soil system with impulsive seismic excitation in bedrock. With the model, he solved for wave responses with time-domain analysis methodology, compared them with MDOF structural modeling with ground excitation, and revealed wave propagation features and influences of soil-structure interaction in seismic structural responses, among others. Todorovska et al. (2001) modeled 2D anisotropic wave propagation for a real seven-story building. While developed over the past decade for exploration seismology, ultrasound and hazard studies, seismic interferometery (SI) was first employed by Snieder et al. (2006a,b) to extract pure structural responses from seismic recordings. This SI methodology was not only used well for explaining wave phenomena in buildings, but also easily for system identification with a 1D uniform shear-beam model. Following Snieders work, Kohler et al. (2007) studied seismic propagating waves in 3D steel, moment-frame building and verified with ETABS finite-element modeling. Recently, SI was further applied for damage detection based on 1D wave traveling times (Todorovska, 2009) and for seismic response analysis with continuous-discrete building models (Zhang et al., 2010 and 2011), among others.

Building upon the aforementioned work as well as pertinent others (e.g., Cai and Lin, 1991; Zhang, 2000), this study proposes one-dimensional seismic wave motion modeling in building structures and examines its effectiveness and broad-based applications.

2. MODELING OF WAVE MOTION IN HIGH RISE BUILDINGS

This section introduces a one dimensional (1D) model to describe propagation of seismic waves in high-rise building structures. For this purpose, this study proposes modeling of an N-story building as a series of shear beams for columns/walls and lumped masses for floors as shown in Figure 1a. Each shear beam is characterized with shear modulus G, mass density ρ, hysteretic damping ratio γ, cross sectional area A, and height h. And each lumped mass is characterized with floor mass m_f and hysteretic damping ratio γ_f. It should be noted that for floor mass computation, overlapped parts with columns/walls at that floor level should be excluded.

For the j^{th} source-free shear beam bounded with $(z_j^-, z_{(j-1)}^+)$, 1D-wave propagation in vertical direction is governed by

$$\frac{\partial^2 u(z,t)}{\partial z^2} = \frac{1}{v_j^2}\,\frac{\partial^2 u(z,t)}{\partial t^2}, \quad for \quad j = 1, 2 \ldots, N \tag{1}$$

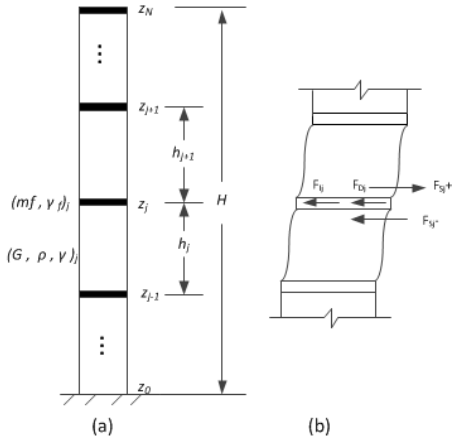

Figure 1. 1D model of N-story high rise building: (a) geometrical configuration; (b) deformed shape at the j^{th} floor.

where $v_j = v_{c_j}(1 + i\gamma_j \ sgn(\omega))$ is the complex velocity of shear waves propagating in the vertical direction where real shear wave velcoicty is given by $v_{c_j} = \sqrt{\frac{G_j}{\rho_j}}$. Introducing Fourier transform pairs of wave motion

$$u(z,t) = \int_{-\infty}^{\infty} U(z,\omega)\, e^{i\omega t}\, d\omega \tag{2}$$

$$U(z,\omega) = \frac{1}{2\pi} \int_{-\infty}^{\infty} u(z,t)\, e^{-i\omega t}\, dt \tag{3}$$

one can solve for shear displacement $u(z,t)$ by substituting Equation 2 into Equation 1 and obtain

$$\int_{-\infty}^{\infty} \left[\frac{\partial^2 U(z,\omega)}{\partial z^2} + \left(\frac{\omega}{v_j} \right)^2 U(z,\omega) \right] \, e^{i\omega t}\, d\omega = 0 \tag{4}$$

Equation 4 can be solved for independent variable z, where general solution can be put in exponential form as $U(z,\omega) = e^{\lambda z}$ in which λ is constant. Then, substituting $U(z,\omega)$ and its derivatives back into Equation 4 yields $\lambda_{1,2} = \mp i\omega/v_j$. Consequently, the general solution of Equation 4 can be given as

$$U_z \equiv U(z,\omega) = C_1\, e^{-i\omega z/v_j} + C_2\, e^{i\omega z/v_j} \equiv \ U_z^u + U_z^d \tag{5}$$

and shear displacement in time domain can then be obtained by substituting Equation 5 back into Equation 2 which results in

$$\begin{aligned} u_z \equiv u(z,t) &= \int_{-\infty}^{\infty} \left(C_1\, e^{i\omega(t - z/v_j)} + C_2\, e^{i\omega(t + z/v_j)} \right) d\omega \\ &= g_1\left(t - z/v_j\right) + g_2\left(t + z/v_j\right) \equiv \ u_z^u + u_z^d \end{aligned} \tag{6}$$

where U_z and u_z are used to represent the compact form of $U(z,\omega)$ and $u(z,t)$ respectively, the superscripts u and d correspond to up-going and down-going propagation directions, and the notation $(\equiv)$ is used to indicate identical quantities.

Equations 5 and 6 can be interpreted physically as the sum of two constant-shape displacement waves travelling in opposite vertical directions with the same velocity, i.e., $C_1 e^{-i\omega z/v_j}$ or $g_1(t - z/v_j)$ propagating upward in the positive z-direction and $C_2 e^{i\omega z v_j}$ or $g_2(t + z/v_j)$ propagating downward in the negative z-direction.

In general, propagating waves are turned into transmitted and reflected waves whenever they encounter a boundary of two different media. Amplitudes of transmitted and reflected waves to amplitude of propagating wave—incident wave—are respectively determined by transmission and reflection coefficients, denoted here as T and R correspondingly. At the j^{th} shear beam bounded with $[z_j^-, z_{(j-1)}^+]$—uniform medium—shown in Figure 2a, propagating waves continue traveling in the same direction without reflection. Mathematically, this means that reflection coefficient, in either direction, is equal to zero. Therefore, out-going and in-going waves can be related through transmission and reflection coefficients and written in a matrix form as

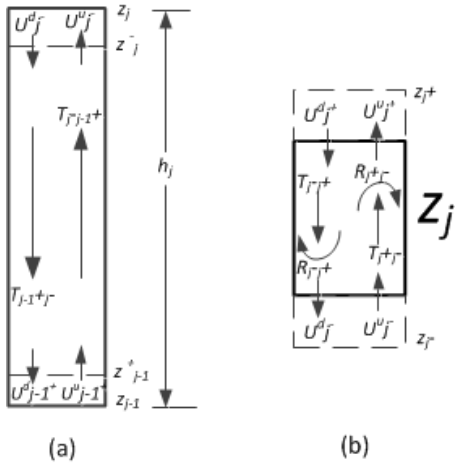

Figure 2. Transmission and reflection coefficients: (a) through the j^{th} shear beam; (b) through the j^{th} lumped mass.

$$\begin{Bmatrix} U^u_{j^-} \\ U^d_{(j-1)^+}) \end{Bmatrix} = \begin{bmatrix} T_{j^-(j-1)^+} & 0 \\ 0 & T_{(j-1)^+ j^-} \end{bmatrix} \begin{Bmatrix} U^u_{(j-1)^+} \\ U^d_{j^-} \end{Bmatrix} \tag{7}$$

from which transmission coefficient can be derived with the aid of Equation 5

$$T_{j^-(j-1)^+} = \frac{U^u_{j^-}}{U^u_{(j-1)^+}} = e^{\frac{-i\omega h_j}{v_j}} = T_{(j-1)^+ j^-} \tag{8}$$

To examine transmission coefficient in time domain, one can perform inverse Fourier transform by applying Equation 2 to Equation 8, which yields

$$\tilde{T}_{j^-(j+1)^+} = \int_{-\infty}^{\infty} e^{-i\omega \frac{h_j}{v_j}} \, e^{i\omega t} \, d\omega = \; B_j \, \delta\,(t - \tau_j) \tag{9}$$

Equation 9 shows transmission coefficient in time domain is a delta function, $\delta(t)$, with time delay $\tau_j = h_j / v_{c_j}$, meaning that up-going impulsive wave propagates upward with frequency-dependent attenuation coefficient given by $B_j = e^{-\gamma_j |\omega| \frac{h_j}{v_{c_j}}}$.

Floor slabs can be assumed infinitely rigid compared to columns/walls at their own planes. Therefore, one can write shear displacement compatibility and dynamic force equilibrium at the j^{th} lumped mass, shown in Figure 2b, as

$$u(z_j^+, t) = u(z_j, t) = u(z_j^-, t) \tag{10}$$

$$F_S(z_j^+, t) - F_S(z_j^-, t) - F_D(z_j, t) = F_I(z_j, t) \tag{11}$$

where the $(+, -)$ sings respectively indicate the up and down sides of the j^{th} lumped mass, and $F_S = GA\ \partial u(z_j, t)/\partial z$ is the shear force resulting from shear deformation at $(j+1)^{th}$ and j^{th} shear beams, and $F_D = c_f\ (z_j, t)/\partial t$ and $F_I = m_f \partial^2 u(z_j, t)/\partial^2 t$ are respectively the damping and inertia forces due to the j^{th} lumped mass motion. For simplicity, shear wave components at each level will be indicated by level notation, i.e., $U_j^u \equiv U_{z_j^+}^u$.

With the aid of Equations 2 and 5, Equations 10 and 11 can be solved in frequency domain, in which out-going and in-going waves at the j^{th} lumped mass can be related through transmission and reflection coefficients, as shown in Figure 2b. This can be expressed compactly in matrix form as

$$\begin{Bmatrix} U_{j^+}^u \\ U_{j^-}^d \end{Bmatrix} = \begin{bmatrix} T_{j^+j^-} & R_{j^-j^+} \\ R_{j^+j^-} & T_{j^-j^+} \end{bmatrix} \begin{Bmatrix} U_{j^-}^u \\ U_{j^+}^d \end{Bmatrix} \tag{12}$$

where the transmission and reflection coefficients shown in Equation 12 can explicitly be described as

$$T_{j^+j^-} = \frac{2}{1 + r_{I_j} - r_{D_j} + i r_{M_j}} \tag{13a}$$

$$R_{j^+j^-} = \frac{2}{1 + r_{I_j} - r_{D_j} + i r_{M_j}} - 1 = T_{j^+j^-} - 1 \tag{13b}$$

$$T_{j^-j^+} = \frac{2 r_{I_j}}{1 + r_{I_j} - r_{D_j} + i r_{M_j}} \tag{14a}$$

$$R_{j^-j^+} = \frac{2 r_{I_j}}{1 + r_{I_j} - r_{D_j} + i r_{M_j}} - 1 = T_{j^-j^+} - 1 \tag{14b}$$

where the coefficients: r_I, r_D, and r_M can be expressed in terms of column impedance ρv, column cross-sectional area A, floor-to-column mass ratio $r_m = m_f/m$, and wave travel time $\tau = h/v$. These coefficients can be determined using the following expressions

$$r_{I_j} = \frac{(\rho v)_{j+1}}{(\rho v)_j} \frac{A_{j+1}}{A_j} \tag{15a}$$

$$r_{M_j} = r_{m_j} \omega \frac{h_j}{v_j} \tag{15b}$$

$$r_{D_j} = \gamma_{f_j}\ r_{M_j} \tag{15c}$$

Up-going transmission coefficient through the j^{th} lumped mass, given by Eqaution 13a, can be expressed as

$$T_{j^+j^-} = B_{f_j} e^{-i\omega \frac{h_{e_j}}{v_{c_j}}} \tag{16}$$

where the transmission amplitude B_{f_j} and equivalent height h_{e_j} can be expressed respectively as

$$B_{f_j} = \frac{2}{\sqrt{(1 + r_{I_j} - r_{D_j})^2 + (r_{M_j})^2}} \tag{17a}$$

$$h_{e_j} = \frac{v_j}{\omega} tan^{-1} \frac{r_{M_j}}{(1 + r_{I_j} - r_{D_j})} \tag{17b}$$

This indicates that lumped floor mass can be treated as a continuum medium, column-type, with equivalent height but with non-zero reflection coefficients.

Transmission and reflection coefficients at free-top and fixed-bottom ends can also be determined using applicable boundary conditions at those levels. The fact that shear forces are zero at the free surface reveals that $U^d_{N^-} = U^u_{N^-}$, meaning that propagating waves approaching the free-surface level will be completely reflected back. Furthermore, considering displacement compatibility at the free-end level noting that no waves are propagating in the vacuum, $v = 0$, one can express upward transmitted wave as $U^u_N = 2U^u_{N^-}$. This shows that at the free top end, transmission and reflection coefficients in the vertical direction are given respectively as $T_{NN^-} = 2$ and $R_{NN^-} = 1$, meaning that up-going waves near the free end will be transmitted to the free end with double amplitude and reflected back with the same motion direction.

At the fixed-bottom end of the model, or at referenced level which could arbitrarily be selected at any level z_r in more general sense, a zero-displacement condition is dominant due to the fact that building's base is stationary at any time, i.e., $U^u_{0^-} = -U^d_{0^-}$. This suggests that down-going waves approaching the model's base are totally reflected upward with an opposite polarity, i.e., 180 degrees out of phase with the down-going waves, where relative impedance at that boundary is equal to infinity, $r_{I_0} = \infty$.

For a composite section bounded with (l, n), as shown in Figure 3a, with intermediate location (m) such that $(l < m < n)$, or using model notation, $((j-1)^+, j^+)$ with (j^-) in between as shown in Figure 2. Repeating use of Equation 12 for (l, m) and (m, n) will lead to representation of transmission and reflection coefficients between (l, n) in terms of those in the two sub-sections, i.e., (l, m) and (m, n).

With the aid of Figure 3b, out-going and in-going waves through the considered section bounded by levels (l, n) can be related through equivalent transmission and reflection coefficients as written in a matrix form, that is

$$\begin{Bmatrix} U^u_n \\ U^d_l) \end{Bmatrix} = \begin{bmatrix} T_{nl} & R_{ln} \\ R_{nl} & T_{ln} \end{bmatrix} \begin{Bmatrix} U^u_l \\ U^d_n \end{Bmatrix} \tag{18}$$

Equivalent transmission and reflection coefficients for the whole section expressed in terms of sub-sections' coefficients can be obtained as

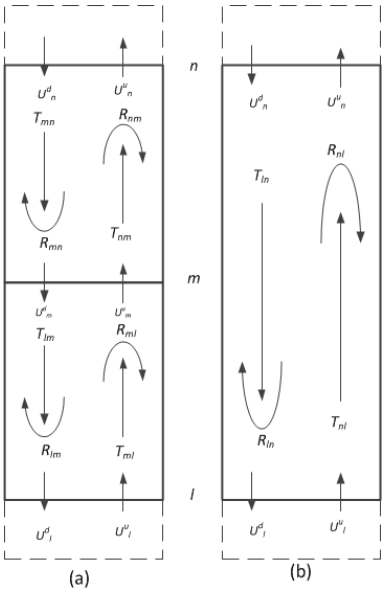

Figure 3. Demonstration of composition rule: (a) sub-segments transmission and reflection coefficients (b) equivalent transmission and reflection coefficients for the whole section.

$$T_{nl} = \frac{T_{ml}T_{nm}}{1 - R_{nm}R_{lm}} \tag{19a}$$

$$R_{nl} = R_{ml} + \frac{T_{ml}R_{nm}T_{lm}}{1 - R_{nm}R_{lm}} \tag{19b}$$

$$T_{ln} = \frac{T_{lm}T_{mn}}{1 - R_{nm}R_{lm}} \tag{20a}$$

$$R_{ln} = R_{mn} + \frac{T_{nm}R_{lm}T_{mn}}{1 - R_{nm}R_{lm}} \tag{20b}$$

The above mentioned composition rule can be applied repeatedly to find all transmission and reflection coefficients between any two levels and ultimately for the whole model.

3. MODEL RESPONSE

Model response in frequency domain can be obtained in non-dimensional form, called hereafter as motion ratio and denoted as $D_{Rr}(\omega)$. Particularly, this response can be determined, at any level, by relating shear displacement at response level, denoted as U_R, to shear displacement at reference level, denoted as U_r. Mathematically the motion ratio can be expressed as

$$D_{Rr}(\omega) = \frac{U_R}{U_r} = \frac{(1 + R_{NR})\, T_{Rr}}{(1 - R_{rR}\, R_{NR})(1 + R_{Nr})} \tag{21}$$

Equation 21 demonstrates that model response is completely dependent on transmission and reflection coefficients of that part of the model which is bounded by reference and free-end levels. Moreover, this formulation proves also that the part underneath the reference level has

no effect on model response, i.e., excludes effects of excitation source, which is not known, as well as soil-structure interaction.

Response representation in time domain can be obtained by applying Fourier transform, given by Equation 2, to model response in frequency domain, given by Equation 21, namely

$$d_{Rr}(t) = \int_{-\infty}^{\infty} D_{Rr}(\omega)\ e^{i\omega t}\ d\omega \tag{22}$$

To understand model response, input/output concept, one can examine model response at $z_R = z_r$, which leads Equations 21 and 22 to 1 and $\delta(t)$ respectively. This means that $D_{Rr}(\omega)$ and $d_{Rr}(t)$ can be interpreted as shear displacement response at response level due to displacement impulse at reference level. Consequently, wave-based representation of model response in terms of shear displacement at z_R to input displacement at z_r is then found as

$$u(z_R, t) = \int_{-\infty}^{\infty} U_R\ e^{i\omega t}\ d\omega = \int_{-\infty}^{\infty} D_{Rr}(\omega)\ U_r\ e^{i\omega t} d\omega \tag{23}$$

$$u(z_R, t) = \int_{-\infty}^{\infty} d_{Rr}(t-\tau)\ u(z_r, \tau)\ d\tau \tag{24}$$

Equations 23 and 24 have the same mathematical form as the traditional vibration response representation in frequency domain with D_{Rr} as frequency response function and in time domain with d_{Rr} as impulse response function, Duhamel's or convolution integral.

While the aforementioned derivation is for displacement input at reference level $(u_r(t), U_r(\omega))$, it is straightforward to extend it to velocity input $(v_r(t) = du/dt, V_r(\omega) = (i\omega)U(\omega))$ and acceleration input $(a_r(t) = d^2u/dt^2, A_r(\omega) = (i\omega)^2U(\omega))$ with D_{Rr} and d_{Rr} remaining the same. For ground acceleration input at z_r and displacement response at z_R, which is the typical case for displacement response to earthquake, Equations 23 and 24 can be modified as

$$u(z_R, t) = \int_{-\infty}^{\infty} H_{Rr}\ A_{z_r}\ e^{i\omega t}\ d\omega \tag{25}$$

$$u(z_R, t) = \int_{-\infty}^{\infty} h_{Rr}\ (t-\tau)\ a(z_r, \tau)\ d\tau \tag{26}$$

where $H_{Rr} = -D_{Rr}/\omega^2$ and h_{Rr} have the conventional meanings for frequency response function and impulse response function respectively. Because of the aforementioned difference, D_{Rr} and d_{Rr} are respectively referred to as wave-based or generalized frequency response function, (GFRF) and generalized impulse response function, (GIRF).

4. IDENTIFICATION OF MILLIKAN BUILDING USING THE RECORDINGS OF YORBA LINDA EARTHQUAKE

This section presents application of parametric identification of Millikan library building, shown in Figure 4, in California with a few number of seismic recordings after the Yorba Linda earthquake of September 3, 2002, shown in Figure 5, using simple-to-complicated wave models.

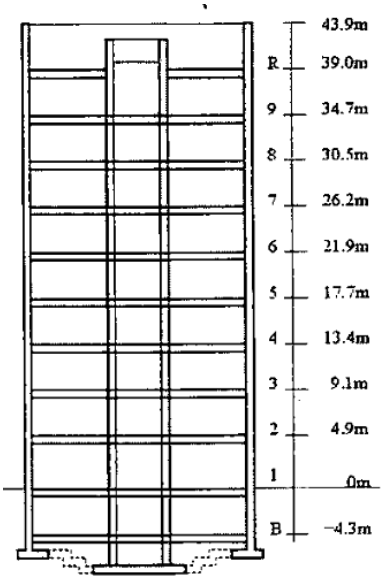

Figure 4. Vertical cross section of the 10-story Millikan Library, Pasadena, California.

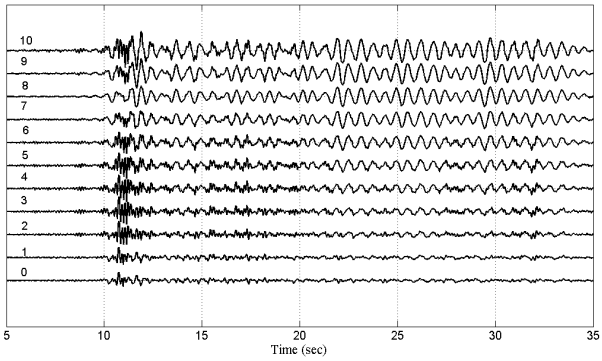

Figure 5. Seismic acceleration recordings of Yorb Linda earthquake in the North-South direction at different floors (indicated as 0 10), where floor levels 0 and 10 correspond to B and R respectively in Figure 4.

For system identification, recording-based GFRF/GIRF is required. One can first calculate the recording-based GFRF as

$$\tilde{D}_{j0}(\omega) = \frac{\tilde{U}_j \tilde{U}_j^*}{|\tilde{U}_j|^2 + \varepsilon} \underset{\varepsilon}{\rightarrow} \frac{\tilde{U}_j}{\tilde{U}_0} \tag{27}$$

where $\tilde{U}$ is the recording in frequency domain, superscript asterisk indicates the complex conjugate, and ε is a positive small number implying the added white noise, which is primarily used to avoid unstable calculation of GFRF at some frequencies near the notches in the spectrum $|\tilde{U}_j|$. As ε approaches zero, $\tilde{D}_{j0}(\omega) = \frac{\tilde{U}_j}{\tilde{U}_0}$, which is Fourier spectral ratio or the definition of GFRF in Equation 21. Note that the tilde over quantities D and U is used to distinguish the recording-based quantities from those based on modeling or Equation 21.

4.1. Parametric Identification with Uniform Shear Beam Model

To capture fundamental dynamic features of the Millikan library, the building can be modeled as uniform shear beam, one-layer, characterized with average properties of the building distributed along the building height. For this case, the model-based GFRF, given by Equation 21, can be written as

$$D_{Rr}(\omega) = \frac{\left(1 + e^{-i\omega\frac{(2H_r - 2z_R)}{v_c}}\, e^{-\gamma|\omega|\frac{(2H_r - 2z_R)}{v_c}}\right) e^{-i\omega\frac{z_R}{v_c}} e^{-\gamma|\omega|\frac{z_R}{v_c}}}{1 + e^{-i\omega\frac{2H_r}{v_c}}\; e^{-\gamma|\omega|\frac{2H_r}{v_c}}} \tag{28}$$

where $H_r = H - z_r$ denotes the height of the building portion bounded by (z_r, z_N). The GIRF can then be found by substituting GFRF of Equation 28 into Equation 22, where the integration can be evaluated with the method of residue. In particular, the integrand for d_{Rr}, a function of the real variable ω, is treated as a function of variable y, which has an infinite number of poles $y_j (j = 1, 2, \dots)$ in the upper half complex plane, namely

$$1 + e^{-iy_j\frac{2H_r}{v_c}}\; e^{-\gamma|y_j|\frac{2H_r}{v_c}} = 0 \Rightarrow y_j = (\pm 1 + i\gamma)\,\omega_j \tag{29}$$

$$\omega_j = \omega_0\,(2j - 1)\,; \qquad \omega_0 = \frac{\pi v}{2H_r}; \qquad for\ j = 1, 2, 3, ...\infty \tag{30}$$

from which the GIRF is obtained as

$$d_{Rr} = 8\omega_0 \sum_{j=1}^{\infty} (-1)^{j+1} e^{-\gamma\omega_j t} cos\left(\omega_j \frac{(H_r - z_R)}{v_c}\right) sin(\omega_j t) \tag{31}$$

Equation 31 shows that d_{Rr} consists of infinite number of motion modes, each of which has exponentially decaying damping factor, modal shape with cosine factor, and sinusoidal motion with modal frequency ω_j. Fundamental or first mode with $j = 1$ has period time given as

$$T_1 = \frac{2\pi}{\omega_1} = 4\,\frac{H_r}{v_c} = 4\tau \tag{32}$$

where τ is the elapsed time for the wave to travel from referenced level to the free-top end. Equation 32 suggests that fundamental period of uniform model equals time elapsed for waves to propagate up and down the height H_r twice.

For parametric identification with a set of three recordings selected at the basement, 3^{rd}, and 8^{th} floors, recordings-based GFRF can be established and fundamental frequency can be determined. With the aid of Equation 30b and the total height of the building, $H = H_r = 48.20$ m, one can find shear wave velocity. Then, hysteretic damping ratio can be determined by applying curve fit optimization with minimizing mean squared error between recordings-based and model-based GFRF which is given by Equation 28 as shown in Figure 6.

With the aid of just obtained model parameters, shear wave velocity and hysteretic damping ratio, one can then get model response in time domain, GIRF, using Equation 31 as shown in Figure 7, which shows model-based GIRF at the 3^{rd} and 8^{th} floors with respect to the basement floor. Obviously, wave features are shown clearly in the early part, $t = 0 \sim$

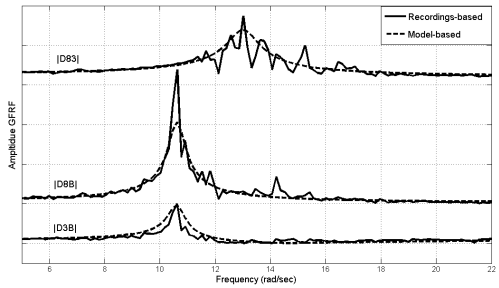

Figure 6. Recording-based GFRF of Yorba Linda EQ at the basement, 3^{rd} and 8^{th} floors with respected to the basement and 3^{rd} floors

$1sec$, exemplified by time shift and amplitude decay as waves propagating up and down the considered levels. At the latter part, vibration features dominant the response, i.e., $t > 1sec$.

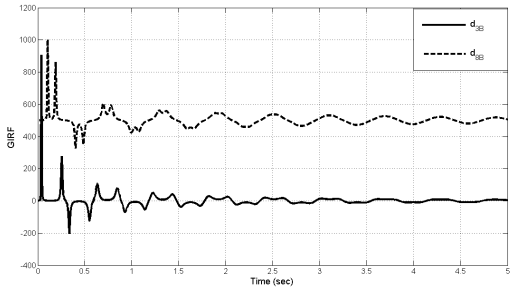

Figure 7. Model-based GIRF at the selected floors: GIRFs at the 3^{rd} and 8^{th} floors with respect to the basement motion using the identified parameters: $H = 48.2\ m$, $v = 326\ m/s$, and $\eta = 0.028$

4.2. Parametric Identification with Piecewise Model

It has been shown that uniform shear-beam model can capture fundamental features of high-rise buildings. However, modeling high-rise buildings as piecewise shear beams could, in principle, more general in characterizing the changing-properties of the structure along the height. To show representation of piecewise model response in frequency domain and time domain, one can examine a simple, two-layer model without floor masses, which leads Equation 21 to

$$\begin{aligned} D_{R0}(\omega) &= \frac{\left[1+\alpha\left(e^{-2i\omega(\tau_1-\tau_2)}\right)+e^{-2i\omega\tau_2}\right)+e^{-2i\omega(\tau-\tau_2}\right]e^{-i\omega\tau_z}}{1+\left[e^{-2i\omega\tau_1}+e^{-2i\omega\tau_2}\right]+e^{-2i\omega\tau}} \\ for \quad 0 \le z \le h_1\ ,\ \tau_z &= \frac{z}{v_1} \end{aligned} \tag{33}$$

$$\begin{aligned} D_{R0}(\omega) &= \frac{2[1+e^{-2i\omega(\tau-\tau_z)}]\frac{e^{-i\omega\tau_z}}{[1+r_{I_1}]}}{(1+\alpha[e^{-2i\omega\tau_1}+e^{-2i\omega\tau_2}]+e^{-2i\omega\tau})} \\ for \quad h_1 \le z \le h_1+h_2\ ,\ \tau_z &= \frac{h_1}{v_1}+\frac{z-h_1}{v_2} \end{aligned} \tag{34}$$

where τ_z is the wave travel time between referenced and response levels. the other parameters are defined as

$$\tau_1 = \frac{h_1}{v_1}, \quad \tau_2 = \frac{h_2}{v_2}, \quad \tau = \tau_1 + \tau_2$$
$$\alpha = \frac{(1 - r_{I_1})}{(1 + r_{I_1})}, \quad r_{I_1} = \frac{(\rho v)_2}{(\rho v)_1} \frac{A_2}{A_1} \tag{35}$$

GIRF, can be found by substituting GFRF of Equations 33 and 34 into Equation 22, where the integration can be obtained in closed form with the method of residues for some special cases and numerically for general cases. Below are presented some special cases, which could help understand the characteristics of wave propagation in buildings and subsequently aid in system identification for general cases.

The denominator of Equations 33 and 34, a function of the real variable ω, is treated as a function of variable y, which has an infinite number of poles $y_j (j = 1, 2 \dots)$ in the upper half complex plane, namely

$$1 + \alpha[e^{-2iy_j\tau_1} + e^{-2iy_j\tau_2}] + e^{-2iy_j\tau} = 0 \tag{36}$$

which can be solved for the variable y_j in a general form as

$$y_j = (1 + i\gamma_{eq})\, \omega_j \quad ; \quad j = 1, 2, \dots, \infty \tag{37}$$

For the case of $\gamma_1 = \gamma_2$ and $\tau_1 = \tau_2$, one can solve the denominator of Equations 33 and 34 for resonant frequencies as

$$\omega_{2j-1} = \frac{[(2j-1)\pi - \beta]}{\tau} \tag{38a}$$
$$\omega_{2j} = \frac{[(2j-1)\pi + \beta]}{\tau} \tag{38b}$$
$$\alpha = \pm cos(\beta) \tag{38c}$$
$$\gamma_{eq} = \gamma_1 = \gamma_2 \tag{38d}$$

and for the case of $r_{I_1} = 1$, which could be, but not necessarily, the uniform or one-layer model, GIRF can be found in the form of

$$d_{Rr} = \frac{4\pi}{\tau} \sum_{j=1}^{\infty} (-1)^{j+1}\, e^{-\gamma_{eq}\, \omega_j (t - \tau_z)}\, cos(\omega_j(\tau - \tau_z))\, sin(\omega_j t) \tag{39}$$

which is consist with Equation 31.

For a set of recordings available at the basement, 4^{th}, and 7^{th} floors, the recording-based GFRF of $\tilde{D}_{40}$ and $\tilde{D}_{70}$ with $\varepsilon = 5\%$ of the total power spectrum of the basement motion is obtained as shown in Figure 8 by the solid line. In principal, all the frequencies corresponding to the spectral peaks, can be regarded as modal frequencies and then used for system identification. For simplicity and in practice as well as for illustration with the use of a two-layer model without floor masses, parametric identification is carried out here based on two modal frequencies identified from Figure 8: $\omega_1 = 10.62\ rad/s$ and $\omega_2 = 14.22\ rad/s$. With the use of Equations $38a \sim c$, the following parameters are found as

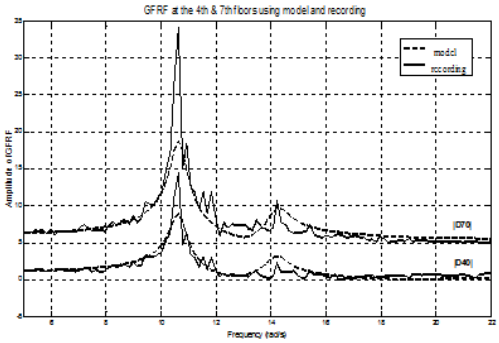

Figure 8. Comparison of GFRF amplitudes at the 4th and 7th floors with respect to impulsive basement acceleration obtained from seismic recordings and model Equation 33.

$$\tau = \frac{2\pi}{(\omega_1 + \omega_2)} = 0.253\ sec$$
$$\beta = \frac{\pi(\omega_2 - \omega_1)}{(\omega_1 + \omega_2)} = 0.455\ rad$$
$$\alpha = Cos(\beta) = 0.898$$

with this in mind, the other model parameters can be determined as:
$r_{I_1} = 0.053$, $v_1 = 361.85\ m/s$, $v_2 = 19.18\ m/s$, $h_1 = 45.77\ m$, $h_2 = 2.43\ m$.

Model-based GFRF with identified parameters and using Equation 33 is indicated in Figure 8 with dashed line. It should be noted that the aforementioned identification is carried out under the special condition of $\gamma_1 = \gamma_2$ and $\tau_1 = \tau_2$. In general, the parameters r_{I_1}, v_1, v_2, h_1 and h_2, together with γ_1 and γ_2, can be found by minimizing mean squared error of the model-based GFRF from recording-based GFRF in certain frequency range $(say\ 5 \sim 22\ rad/s)$, among many other identification algorithms. Figure 9 shows the comparison of recording-based GIRF at the 7^{th} floor with respect to band-limited $(\varepsilon = 5\%)$ impulsive motion at the basement against model-based counterparts with respect to pure $(\varepsilon = 0\%)$ impulsive motion at the basement.

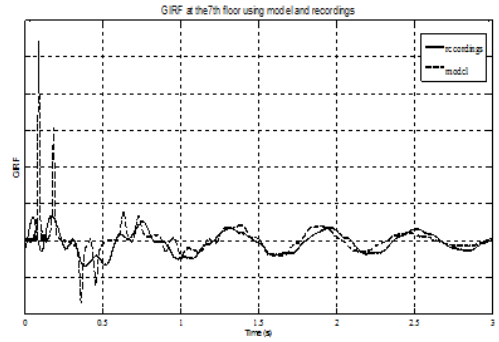

Figure 9. Comparison of GIRF at the 7th floor with respect to basement acceleration motion obtained from seismic recordings and model.

4.3. Parametric Identification with Continuous-Discrete Model

In general, the more number of degrees of freedom used for the building system, the more robust the model is. For the Millikan library building, it can be modeled as continuous-discrete system, where floor heights are obtained from the vertical cross section shown in Figure 4. Model parameters are estimated based on seismic recordings provided at the basement and 8^{th} floors. System identification in this case is carried out based on numerically minimizing the mean squared difference of recorded-based GFRF from model-based GFRF. For instance, two sets of modal frequency are considered here for system identification, i.e., $(10.62, 11.82)\ rad/s$ and $(10.62, 13.46, 14.21)\ rad/s$, which are shown graphically in Figures 10 and 11 respectively.

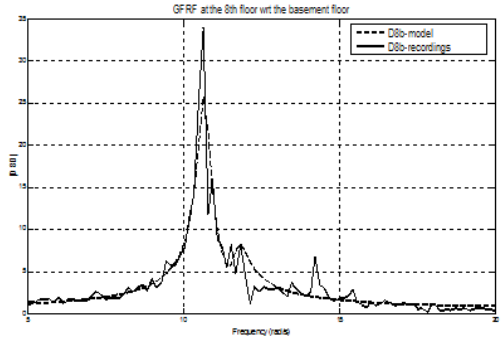

Figure 10. System identification using seismic recordings at the basement and 8^{th} floors with continuous-discrete model matching two modal frequencies at 10.62 and 11.82 rad/sec.

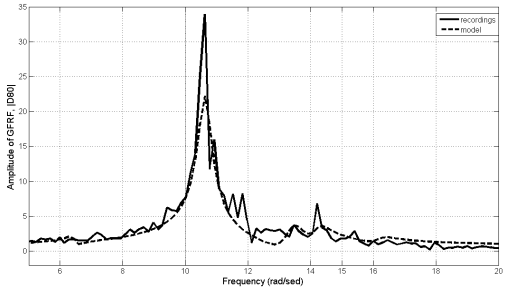

Figure 11. System identification using seismic recordings at the basement and 8^{th} floors with continuous-discrete model matching three modal frequencies at 10.62, 13.46, and 14.21 rad/sec.

Model parameters identified from the the above system identification are summarized in the table below

5. STOCHASTIC ANALYSIS OF MATERIAL/GEOMETRICAL INFLUENCE ON WAVE-BASED RESPONSE

This section presents analysis of influence of model parameters on wave-based response. Among the important factors to be analyzed and discussed are mass ratio, r_m and impedance ratio, r_I. Equations 13a and 14a show that as mass ratio increases, the amplitude

Table 1. Modal parameters identified using recordings

Modal-frequency set (rad/sec)	Discrete mass ratio r_m	Shear wave velocity v (m/s)	Impedance ratio r_I	hysteretic damping ratio (γ, γ_β)
(10.62,11.82)	r_{m_j}=0.65, j=1:10 $r_{m_{11}}$=0.50 r_{m_j}	v_j=360, j=1:9 v_j=67, j=10,11	r_{I_j}=1,1:8 r_{I_9}=0.0065 $r_{I_{10}}$=0.43	γ, γ_β=0.025
(10.62, 13.46,14.21)	r_{m_j}=0.70, j=1:10 $r_{m_{11}}$=0.50 r_{m_j}	v_j=355, j=1:8 v_9=14.35 v_j =13.8,j=10,11	r_{I_j}=1,1:7 r_{I_8}=0.15 r_{I_9}=0.85 $r_{I_{10}}$=0.43	γ, γ_β =0.02

of up-going and down-going of propagating waves through lumped mass decreases, for the given relative and hysteretic damping ratios. This suggests that waves will reach to the higher levels of the building with small amplitudes, or less energy. For cases of small mass ratios, however, one can simplify the continuous-discrete model to a piecewise/uniform model which can be explained as detailed below.

For most ordinary and regular high-rise buildings, one can consider that wave-based model characteristics, such as shear wave velocity v, shear area A, column impedance v, and column height h, are not changed significantly from floor to floor. Practical design consideration of high-rise buildings subjected to earthquake-related excitation motion regards that the largest dominant frequency of interest, $\tilde{\omega}_{max}$ is typically less than $n\omega_1$ with $n < N$. Mathematically, this can be put in the form below

$$r_{M_j} = r_{m_j} \frac{h_j}{v_j} \tilde{\omega}_{max} < r_{m_j} \frac{h_j}{v_j} n\omega_0 \tag{40}$$

with the Equation 31b and assuming that $H = Nh_j$, Equation 40 can be written as

$$r_{M_j} < r_{m_j} \frac{\pi}{2} \frac{n}{N} \ll 1 \tag{41}$$

Based on Equation 41, the quantities r_{M_j} and r_{D_j} can practically be approximated to zero. Consequently, one can conclude that transmission and reflection coefficients, given by Equations 13 and 14, in this case are functions only of impedance ratio. This clearly shows that under the considered condition of small floor-to-column mass ratio, the continuous-discrete mass model can be degenerated to piecewise model. To examine effect of mentioned simplification on dynamic features of the reduced model, one can apply small-angle approximation to Equation 17b, that is

$$h_{e_j} \approx \frac{v_j}{\omega} \frac{r_{M_j}}{(1 + r_{I_j})} \approx \frac{r_{m_j}}{(1 + r_{I_j})} h_j \tag{42}$$

Equation 42 demonstrates that lumped mass at the j^{th} level functions like an extended height over the column segment. Consequently, upward transmission coefficient through the j^{th} column connected to floor mass can be viewed as equivalent to either transmission coefficient in pure column without floor mass but with increased height, or transmission coefficient in pure column with reduced velocity, this can be expressed mathematically as

$$T_{j^+j^-} \approx \frac{2}{(1+r_{I_j})} e^{-i\omega \frac{h_{e_j}}{v_j}} \approx \frac{2}{(1+r_{I_j})} e^{-i\omega \frac{h_j}{v_{e_j}}} \tag{43}$$

where $v_{e_j} = v_j/(1 + r_{m_j}/2)$. In this case, the impedance ratio given by Equation 15a can be approximated to one for $j = 1, 2 \ldots, N-1$. Consequently, upward and downward transmission coefficients given by Equations 13a and 14a can be written in the following form

$$T_{j^+j^-} \approx T_{j^-j^+} \approx e^{-i\omega \frac{h_{e_j}}{v_j}}, \quad j = 1, 2, N-1 \tag{44}$$

which suggests that upward and downward propagating waves through thej^{th} floor are transmitted with constant amplitude and zero reflection.

Accordingly, the fundamental frequency and fundamental period of continuous-discrete-mass model, denoted as Ω_0 and T_1, are respectively less than and higher than the fundamental frequency and fundamental period of the same model without lumped masses, uniform model, ω_1 and τ_0.

For high-order mode motion $(j > 1)$, the modal frequencies Ω_j of the building with floor masses will be reduced proportionally and the corresponding amplitude will be increased in general. The mean μ and standard variation σ of modal frequency Ω_j can be found as

$$\mu_{\Omega_j} = \omega_j(1 - 0.5\ \mu_{r_m}) \tag{45a}$$

$$\sigma^2_{\Omega_j} = 0.25\ \mu^2_{\Omega_j} \sigma^2_{r_m} \tag{45b}$$

where μ_{r_m} and σ_{r_m} are the mean and standard deviation of random floor-to-column mass ratio. It can be proved that if $r_{m_j}, (j = 1, 2, ..., N)$, is constant and floor height h_j is random, Equations 45 remains the same except μ_{r_m} and σ_{r_m} replaced by μ_h and σ_h respectively. The other statistical responses such as mean and standard deviation of frequency response amplitudes at corresponding modal frequencies can be found numerically based on Equations 28, 32, and 45.

For large floor-to-column mass ratio or other random system parameters, the statistical analysis for GIRF/GFRF must be carried out numerically or with Monte Carlo simulation. While not presented here, this paper shows influences of some system parameters in frequency responses. In particular, Figure 12 shows the influences of large floor-to-column mass ratio $(r_{m_j} = 1)$ in GFRF, revealing similar phenomena observed with small r_{m_j} before. Figure 13 indicates that modal frequencies are insensitive to the change of column impedance ratio r_I, while the corresponding amplitudes are reduced significantly with decreased r_I.

For ground motion characterized by stationary stochastic process (Lin and Cai, 1995)

$$a(z_0, t) = \int_{-\infty}^{\infty} e^{i\omega t} dZ(\omega) \tag{46}$$

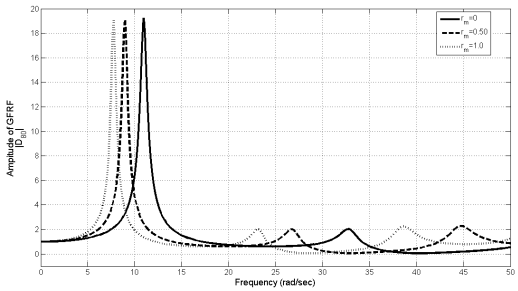

Figure 12. GFRFs (D_{8b}) at the 8^{th} floor of a 11-story building with respect to bottom motion with $v_j = 300\ m/sec$, $h_j = 4.25\ m$, $\gamma_j = \gamma_{f_j} = 0.03$, $r_{I_j} = 1$, and $r_{m_{11}} = 0.5r_{m_j}$, for $j = 1, 2 \ldots, 11$.

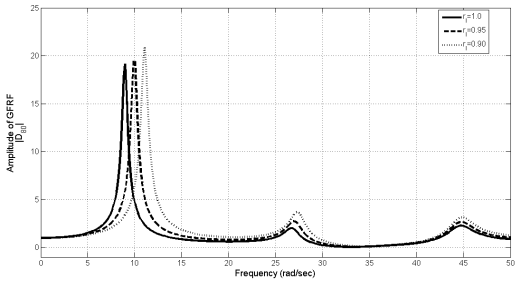

Figure 13. GFRFs (D_{8b}) at the 8^{th} floor of a 11-story building with respect to bottom motion with $v_j = 300\ m/sec$, $h_j = 4.25\ m$, $\gamma_j = \gamma_{f_j} = 0.03$, $r_{m_j} = 0.50$ and $r_{m_{11}} = 0.5\mathrm{r}_{m_j}$, with different values of impedance ratio, for $j = 1, 2 \ldots, 11$.

where Z is a stochastic process with orthogonal increment in frequency, the mean square acceleration response with deterministic building parameters can be found as

$$E[a^2(z,t)] = \int_{-\infty}^{\infty} \Phi(\omega)\ d(\omega) \tag{47a}$$

$$\Phi(\omega) = D_{R0}^2(\omega)\ G(\omega) \tag{47b}$$

where E denotes ensemble average, and G and Φ are spectral densities of ground acceleration and response respectively. For Kanai-Tajimi spectrum selected for the stochastic ground motion characterization, i.e.,$G(\omega) = G_0(1 + 4\xi^2\omega^2/\omega_g^2)/[(1 - \omega^2/\omega_g^2)^2 + 4\xi^2\omega^2/\omega_g^2]$, Figure 14a shows the spectral densities of acceleration at the 8^{th} floor with seismic input at alluvium and rock sites. Since the rock predominant frequency ($\omega_g = 27\ rad/s$) is closer to the second modal frequency ($\omega_2 \sim 22 rad/s$) than the alluvium one ($18.4\ rad/s$), the peak with rock at the second modal frequency is larger than that with alluvium. This can also be seen with mean square accelerations 0.0076 and 0.026 m^2/s^4 for rock and alluvium respectively. Figure 14b shows the response spectral densities with different floor-to-column mass ratio, with corresponding mean squares 0.0188, 0.0102, and 0.0076 m^2/s^4 respectively for r_{m_j}= 0, 0.1, and 1.

While the aforementioned approach to calculate statistical responses to stochastic ground motion is widely used for seismic design and analysis, it is of interest to note some differences from the conventional one. First, the response calculated in this study is absolute

acceleration, not the relative displacement in traditional approach, although they are obtainable from one to the other. More important, the traditional approach assumes that the building is fixed on the ground and subsequently shakes under seismic free-field ground motion, the latter of which is typically characterized by KanaiTajimi model with predominant frequency (ω_g) and damping (γ_g) for site amplification. In fact, for a building fixed on the ground, the seismic input at the fixed bottom of a building is the response of soilstructure interaction, not simply the free-field motion. The Fourier spectrum of basement motion showing that the motion has no clear predominate frequency. This suggests that either the seismic input in traditional approach needs modified as other type such as band-limited white noise for this case, or the fixed boundary condition is inappropriate. By contrast, this model shows that as long as a motion recording at given location (either at ground or one height) is provided, the statistical response at other location can be obtained.

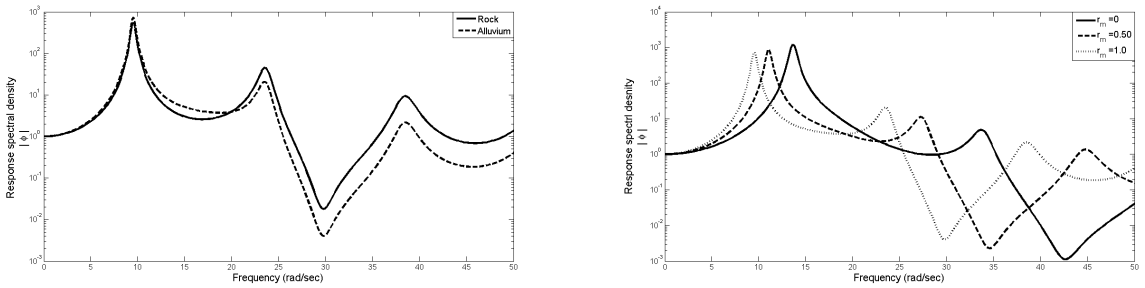

(a) $(\omega_{g_{rock}} = 27, \omega_{g_{allivium}} = 18.4)\ rad/sec$, $r_{m_j} = 1.0$ (b) $\omega_{g_{allivium}} = 18.4$, $r_{m_j} = 0, 0.50, 1.0$

Figure 14. Spectral density of acceleration at the 8^th floor to ground acceleration spectral density with Kanai-Tajimi power spectra (G_0=1), site predominant frequency ω_g, site damping $(\xi_g = 0.34)$, with the same building parameters as indicated in Figure 12

6. CONCLUSION

This study proposes a wave-based approach to model and analyze seismic building motion. It first derives the generalized impulse and frequency response functions (GIRF and GFRF) which are fundamentally important in constructing response to the motion input to a system, not the traditional force input. The deterministic and stochastic features of GIRF and GFRF as well as seismic response are also examined in detail, revealing not only well-observed vibration features of building structures, but also some perspective of seismic wave behaviors of structures which traditional vibration-based approach does not show clearly. While this study focuses on one-dimensional wave propagation with specific shear-beam model for columns/walls and lumped mass for floor, it can be extended to sophisticated modeling such as bending-moment beam model for columns with one extra dimensional wave motion, or another dimension in rocking. While this extension will make the modeling more robust and useful in broad-based applications, the analysis and fundamental features of wave propagation will remain the same as revealed in this study.

7. ACKNOWLEDGMENTS

This work was supported by the Colorado School of Mines Petroleum Institute joint research project under the auspices of Abu Dhabi National Oil Company. The opinions, findings and conclusions expressed herein are those of the authors and do not necessarily reflect the views of the sponsors.

8. REFERENCES

[1] Kohler MD, Heaton TH, Bradford SC., "Propagating waves in the steel, moment-frame factor building recorded during earthquakes. *Bulletin of the Seismology Society of America.* 97(4), 1334-45, 2007.

[2] Safak E., "Wave-propagation formulation of seismic response of multistory building. *Journal of Structural Engineering, ASCE* 125(4), 426-37, 1999.

[3] Snieder R., Safak E., "Extracting the building response using seismic interferometry: theory and application to the Millikan library in Pasadena, California. *Bulletin of the Seismology Society of America.* 96(2), 586-98, 2006.

[4] Snieder R., Sheiman J., Calvert R., "Equivalence of virtual-source method and wave-field deconvolution in seismic interferometry. *Physical Review 2006.*E73:066620(9pages).

[5] Todorovska MI., Ivanovic SS., Trifunac MD., "Wave propagation in a seven-story reinforced concrete building I: Theoretical models. *Soil Dynamics and Earthquake Engineering*21, 21123, 2001.

[6] Cai GQ, Lin YK., "Localization of wave propagation in disordered periodic structures. *AIAA Journal*29(3), 450-6, 1991.

[7] Lin YK., Wu WF., "A closed form earthquake response analysis of multistory building on compliance soil. *Journal of Structural Engineering*12(1), 87-110, 1984.

[8] Zhang R.,Yong Y., Lin YK., "Earthquake ground motion modeling. I: Deterministic point source and II: Stochastic line source.. *Journal of Engineering Mechanics-ASCE* 117, 2114-32 and 2132-50, 1991.

[9] Zhang R., "Some observations on modeling of wave motion in a layer-based elastic medium. *Journal of Sound and Vibration* 229(5), 1193-1212, 2000.

[10] Chopra A. "Dynamics of structures-theory and applications to earthquake engineering. *Prentice-Hall,Inc* , 1995.

[11] Lin YK, Cai GQ, "Probabilistic structural dynamics-advanced theory and applications. *McGraw-Hill,Inc* 229(5), 1995

[12] Zhang, R., S. Al Hilali, A. Abdulla, and M. Al Kurbi, "A Wave-based Approach for Seismic Response Analyses of High-Rise Buildings. *proceedings of the IUTAM Symposium (International Union for Theoretical and Applied Mechanics)* Vol. 29, Nonlinear Stochastic Dynamics and Control (Zhu, Lin and Cai, eds.), 336-346, ISBN: 978-94-007-0731-3, 2010

[13] Zhang, R., R. Snieder, L. Gargab and A. Seibi, "Modeling of seismic wave motion in high-rise buildings. *Probabilistic Engineering Mechanics* 25, 520-527, 2011